NJC

Accepted Manuscript

This is an *Accepted Manuscript*, which has been through the Royal Society of Chemistry peer review process and has been accepted for publication.

Accepted Manuscripts are published online shortly after acceptance, before technical editing, formatting and proof reading. Using this free service, authors can make their results available to the community, in citable form, before we publish the edited article. We will replace this *Accepted Manuscript* with the edited and formatted *Advance Article* as soon as it is available.

You can find more information about *Accepted Manuscripts* in the Information for Authors.

Please note that technical editing may introduce minor changes to the text and/or graphics, which may alter content. The journal's standard Terms & Conditions and the Ethical guidelines still apply. In no event shall the Royal Society of Chemistry be held responsible for any errors or omissions in this *Accepted Manuscript* or any consequences arising from the use of any information it contains.

ROYAL SOCIETY OF CHEMISTRY

www.rsc.org/njc

New Journal of Chemistry RSCPublishing

ARTICLE

Slow magnetic relaxation and photoluminescent properties of a highly coordinated erbium(III) complex with dibenzoylmethane and 2,2'-bipyridine

Cite this: DOI: 10.1039/xoxxoooooox

Received ooth January 2012,
Accepted ooth January 2012

DOI: 10.1039/xoxxoooooox

www.rsc.org/

Pablo Martín-Ramos,[a,b] Joana T. Coutinho,[c] Manuela Ramos Silva,[a*] Laura C.J. Pereira,[c] Fernando Lahoz,[d] Pedro S. Pereira da Silva,[a] Víctor Lavín[d] and Jesús Martín-Gil[b]

A new Er(III) β-diketonate complex, tris(dibenzoylmethanate)mono(2,2´-bipyridine) erbium(III) or [Er(dbm)$_3$(bipy)], has been synthesized and its structural, thermal, photophysical and low temperature magnetic properties have been characterized. In the new complex, Er(III) ions are coordinated by six O atoms and two N atoms in a distorted square antiprismatic geometry. The Er(III) complex exhibits out-of-phase ($\chi_M^{"}$) ac susceptibility signals, when a static magnetic field is applied, signaling that at zero field a quantum tunneling regime occurs. The nearly semi-circular and symmetrical shape of the Cole-Cole plots sustain the existence of a single magnetic relaxation process. The solid state luminescent studies show an intense, sharp and narrow emission band in the near infrared region. The combined results demonstrate the ability of dbm and bipy to provide an environment that yields both interesting magnetic and optical properties.

Introduction

The electronic, magnetic and photophysical properties of Ln^{3+} complexes strongly depend on the control of the coordination sphere of the lanthanide. Amongst the synthetic strategies developed during the last decades aimed at designing a convenient chemical environment and satisfying the design requirements of each particular application[1] (which include linear polydentate and multifunctional ligands, macrocyclic receptors and podates and self-assembled structures), β-diketonates have been proven to be one of the most popular choices. Apart from their large commercial availability, they have been shown to provide efficient sensitization by the so-called *antenna effect*[2] and lead to complexes with good thermal stability, good processability and thin-film forming properties.[3] In the particular case of erbium(III), one of the most handy options has been dibenzoylmethane or 1,3-diphenyl-1,3-propanedione. Back in 2001 Kawamura *et al.*[4] reported two erbium(III) complexes with dibenzoylmethane as the first ligand and the diimine molecules bathophenanthroline (bath) and phenanthroline (phen) as second ligand which resulted highly efficient as NIR-emitters. Later on, these materials (and other DBM-based complexes) have been shown to be suitable for doping hybrid materials aimed at optical waveguides[5] and as active-layer materials for NIR-OLEDs.[6]

Recently another interesting property of erbium(III) β-diketonate complexes was revealed: their Single-Ion Magnet (SIM) behavior.[7] The same ligands that originate the *antenna effect* create an environment around the lanthanide that originates an energy barrier to spin rotation. It is the ligand field that separates the (2J+1)-fold degenerate multiplets of the Er^{3+} ions, created by the spin-orbit coupling. Complexes with a single lanthanide ion have been found to exhibit energy barriers higher than the more studied *3d* metal Single Molecule Magnets (SMM) complexes.[8] As tiny independent magnets, SIMs and SMMs could be used for high-density information storage but even more interesting they are being considered for quantum computing purposes, namely to build dense and efficient memory devices based on the Grover algorithm.[9]

The combination of two or more properties may also be useful. While the design and study of multifunctional materials have attracted a great deal of attention, analogous efforts regarding multifunctional molecule-based materials combining magnetism and luminescence have been comparatively few in number.[10] In terms of applications, bi-functional or multifunctional materials are usually put forward as potential sensors.[11] Nevertheless, other uses can also be envisioned: for instance, Coronado *et al.* reported the formation of a metal–organic framework (MOF) with nodes that have SIM behaviour. The porous structure allowed the incorporation of

polyoxometalates through anion exchange and was proposed to be used in quantum devices.[12]

Herein we present the work developed from the use of dibenzoylmethanate and bipyridine to coordinate the Er^{3+} ion, searching for aforementioned bifunctionality. We report the structural, thermal, spectroscopic, luminescent and magnetic properties of tris(dibenzoylmethanate)mono(2,2´-bipyridine)erbium(III).

Results and discussion

Synthesis

From a Chemistry point of view, in order to design a convenient chemical environment for the luminescent lanthanide ion, several requirements have to be taken into account. In brief, the first one is a chemical constraint in that the coordination cavity should provide enough donor atoms to saturate the coordination number requirement of the Ln^{3+} ion as well as a large bonding strength ensuring a good thermodynamic stability and possibly also kinetic inertness. The second requirement pertains to the efficiency of the sensitization process, i.e., the energy level scheme of the ligands should be such that it maximizes the energy transfer path: for efficient lanthanide ion sensitization, the triplet states of the ligand must be closely matched to, or slightly above, the metal ion's emitting resonance levels. Thirdly, the antenna ligand excitation wavelength should be above 350 nm to facilitate the use of inexpensive excitation sources and to avoid the use of expensive quartz optics, and –finally- a short distance between the sensitizer and the Ln^{3+} cation is also required in order to ensure fast energy transfer. Consequently, we decided to construct the new Er^{3+} complex by employing a primary (dbm) and a secondary ligand (bipy) which would fulfill all aforementioned requirements. Tris(dibenzoylmethanate)mono(2,2´-bipyridine)erbium(III), both solvated and unsolvated forms, were obtained by mixing erbium nitrate hydrated with dibenzoylmethane (1:3 mmol) in methanol. Potassium methoxide was used to induce potassium nitrate precipitation. The salt was removed by decanting and finally 2,2'-bipyridine (1 mmol) was added. The mixture was heated to 75 ºC and stirred overnight, then washed with dioxane, and finally dried in vacuum to give the product in a high yield.

Crystals suitable for X-ray analysis were obtained by slow evaporation of a methanol-dioxane solution at room temperature but never in a concomitant way. Different batches yielded different crystalline forms as confirmed by X-ray powder diffraction.

Structural description

$[Er(dbm)_3(bipy)]$ crystallizes in a monoclinic unit cell with the $P2_1/c$ space group. The unit cell contains four complexes (Figure 1, Table 1). Within each complex, the Er^{3+} ion is coordinated in a distorted square-antiprismatic geometry by six O atoms from the dibenzoylmetanate anions and two N atoms from the 2,2´-bipyridine molecule. The trivalent erbium ion lies approximately in the middle of the antiprism with a distance of 1.37 Å to the face containing the N atoms and 1.17 Å to the opposite face containing exclusively oxygen atoms. The angle between the least-squares planes of the square faces is 2.07(9)º. The Er–N distances are 2.545(2) and 2.566(2) Å and the Er-O distances lie in the range 2.2402(18)-2.3079(18) Å. The N–Er–N bite angle is 62.86(9)º. Selected geometric parameters are given in Table 2. The chelating rings are approximately planar. The crystal structure is stabilized by C-H…π and π...π interactions.

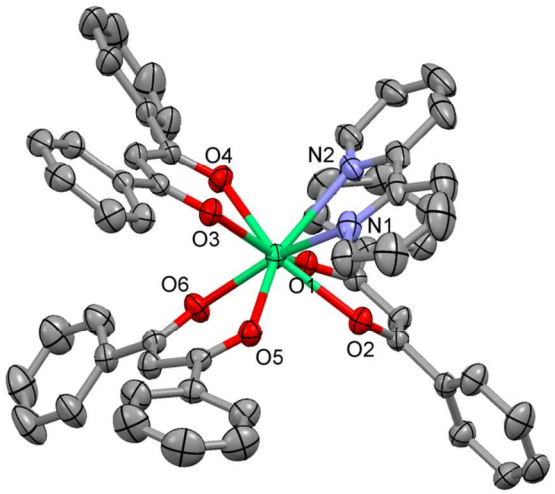

Figure 1. A perspective view of the eightfold coordination of $[Er(dbm)_3(bipy)]$. Displacement ellipsoids are drawn at the 30% probability level. Hydrogen atoms were omitted for clarity.

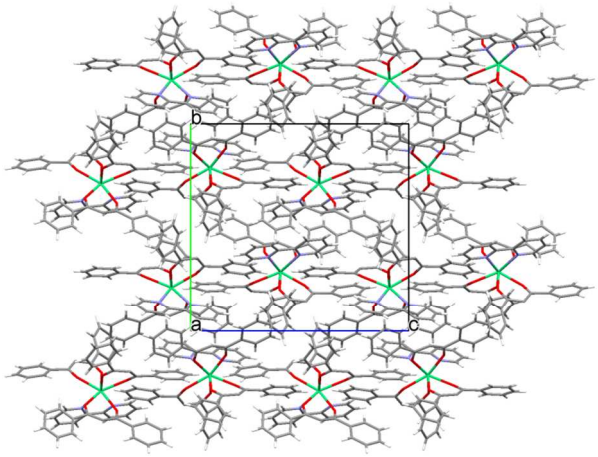

Figure 2. Packing diagram of $[Er(dbm)_3(bipy)]$

A solvated form of $[Er(dbm)_3(bipy)]$ crystallizes in a triclinic unit cell with the *P*-1 space group. The unit cell contains four complexes. Within each complex, the Er^{3+} ion is coordinated in a distorted square-antiprismatic geometry by six

O atoms from the dibenzoylmethanate anions and two N atoms from the 2,2'-bipyridine molecule.

The solvent molecules (probably 1,4-dioxane) are disordered in the crystal and the resulting electron density was found to be uninterpretable. The solvent contribution to the structure factors was taken into account by back-Fourier transformation of all density found in the disordered solvent area using the SQUEEZE routine in PLATON.[13] The formula mass and density do not take the solvent into account.

To find out the degree of distortion of the square antiprism, the Φ and α angles were calculated (Figure 3). Φ is the skew angle, with an ideal value of 45° for a regular square antiprism.[14] For our distorted polyhedron, Φ was calculated by projecting Er1, N1, N2, O3 and O4 to the mean plane of the most regular face (O1, O2, O5, O6) and then calculating the angles between the projected vectors. α (defined as the angle between the C_4 axis and the Er–O,N direction) was calculated by considering the direction between Er1 and the centroid of the (O1, O2, O5, O6) square face as the C_4 axis and then computing the angle between this axis and the Er–N,O vectors. The total sums of the deviation from the ideal values for Φ and α are 73.9° and 40.3°, respectively. These values are larger than those observed for [Er(h)$_3$(bipy)] [36.2º; 30.3º][7a], for [Er(tfa)$_3$(bipy)] [50.0º; 28.0º], or for [Er(tpm)$_3$(bipy)] [56.4º; 27.8º].[7c]

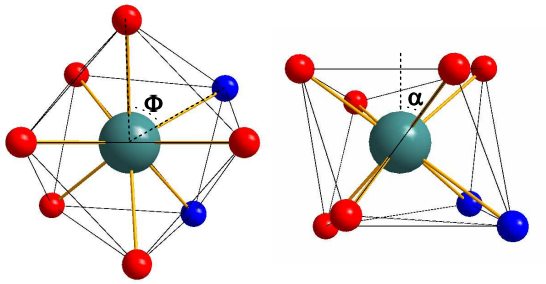

Figure 3. Definition of Φ and α in the square-antiprismatic geometry.

X-ray powder diffraction

Figure 4 shows the experimental diffraction pattern and the simulated powder diffraction pattern from the single crystal structure using PLATON.[13] There is a good match between simulated and experimental diffractograms: the peaks appear at the predicted theta angles. Differences in intensity are related to the Bragg-Brentano geometry of the diffractometer.

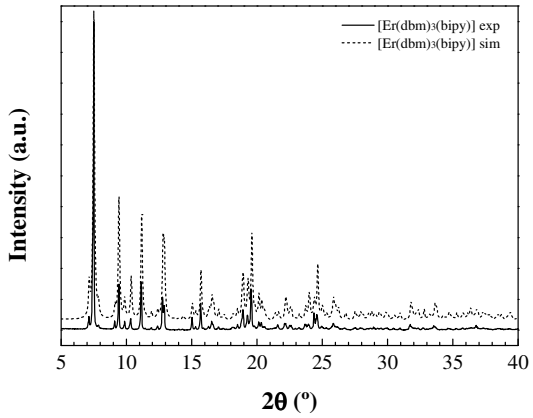

Figure 4. Experimental (*solid line*) *vs*. simulated (*dashed line*) X-ray powder diffraction pattern for [Er(dbm)$_3$(bipy)].

New Journal of Chemistry RSCPublishing

ARTICLE

Table 1. Crystal data and structure refinement for $[Er(dbm)_3(bipy)]$ and its solvated form

Complex	$[Er(dbm)_3(bipy)]$	Solvated $[Er(dbm)_3(bipy)]$ form
Empirical formula	$C_{55}H_{41}ErN_2O_6$	$C_{55}H_{41}ErN_2O_6$
Formula weight	990.13	990.13
Temperature (K)	293(3)	293(2)
Wavelength (Å)	0.71073	0.71073
Crystal system	Monoclinic	Triclinic
Space group	$P2_1/c$	*P-1*
a (Å)	14.9946(6)	15.2886(6)
b (Å)	17.0429(7)	17.7424(7)
c (Å)	22.7907(8)	20.7735(7)
α (º)	90	73.910(3)
β (º)	128.291(2)	70.046(2)
γ (º)	90	68.647(3)
Volume (Å^3)	4571.3(3)	4857.3(3)
Z	4	4
Calculated density (g cm^{-3})	1.443	1.358
Absorption coefficient (mm^{-1})	1.899	1.778
F(000)	2004	2004
Crystal size (mm^3)	0.33×0.18×0.18	0.15×0.08×0.07
θ range for data collection	2.10-25.66º	2.50-25.82º
Index ranges	-18<*h*<18; -20<*k*<20; -27<*l*<27	-18<*h*<18; -21<*k*<21; -25<*l*<25
Reflections collected	82332	93128
Independent reflections	8649	7635
Completeness to 2θ=51º	99.9%	99.4%
Refinement method	Full matrix LS on F^2	Full matrix LS on F^2
Data/restrains/parameters	8649/0/577	18606/19/859
Goodness-of-fit on F^2	1.058	0.870
Final *R* indices [$I>2\sigma(I)$]	*R*=0.0208; w*R*=0.0499	*R*=0.0664; w*R*=0.1354
R indices (all data)	*R*=0.0334; w*R*=0.0513	*R*=0.1672; w*R*=0.1627
Largest diff. peak and hole	0.399/-0.284	0.949/-0.786

Table 2. Selected distances and angles (Å,º) for $[Er(dbm)_3(bipy)]$

Bond	Distance	Bonds	Angle
Er1-N1	2.565(2)	O1-Er1-O2	72.94(6)
Er1-N2	2.546(2)	O2-Er1-O5	76.48(6)
Er1-O1	2.2970(16)	O5-Er1-O6	73.64(6)
Er1-O2	2.3064(16)	O6-Er1-O1	77.25(6)
Er1-O3	2.2962(16)	O1-Er1-O5	128.75(6)
Er1-O4	2.3077(16)	O2-Er1-O6	106.94(6)
Er1-O5	2.3062(16)	O3-Er1-O4	72.13(6)
Er1-O6	2.2395(16)	O3-Er1-N1	76.81(6)
Er1-N avg.	2.556	O4-Er1-N2	73.59(7)
Er1-O avg.	2.292		

Thermal analysis by DSC

No significant thermal effects could be discerned up to 350 ºC, neither in sealed nor in perforated aluminum pans (two of these later runs are shown in Figure 5). This is in agreement with the good thermal stabilities reported for similar Eu^{3+} complexes.[15] Nevertheless, it should be noted that, upon aperture of the pans, some degradation had occurred: the color of the samples had evolved from light pink to brown. Further, a 15% mass loss was confirmed in the perforated pans, which would be in agreement with the loss of the 2,2'-bipyridine ligand (which accounts for 15.72% of the M_W), in accordance to DTA studies conducted by Zhou *et al.* for Eu^{3+} complexes.[16] The beginning of this degradation can be tentatively associated to a very weak endothermic effect at ca. 230 ºC.[16] Overall, the complex can be regarded as thermally stable enough to be used in molecular devices.

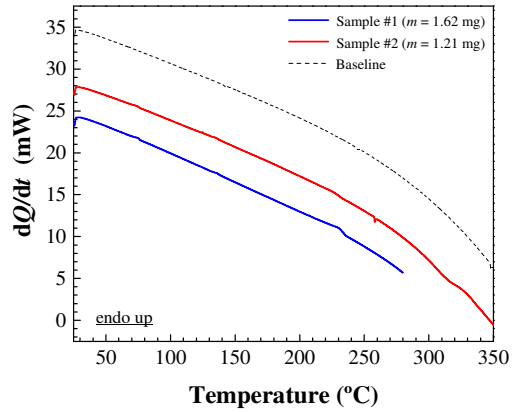

Figure 5. DSC curve of [Er(dbm)$_3$(bipy)] complex.

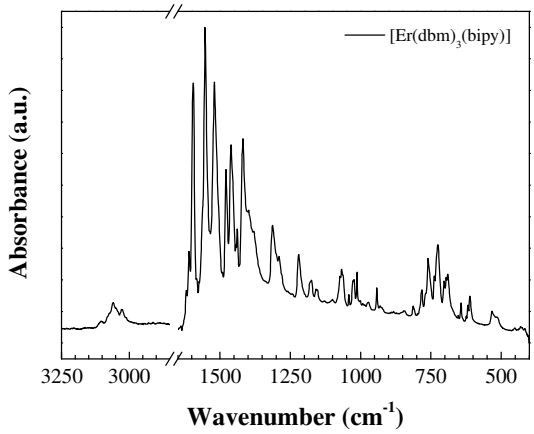

Figure 6. ATR-FTIR spectrum of [Er(dbm)$_3$(bipy)] complex.

Vibrational characterization

Infrared spectrum

The ATR-FTIR spectrum of [Er(dbm)$_3$(bipy)], corrected using ThermoScientific OMNIC™ software, is shown in Figure 6. Absorption bands in the FTIR (and Raman) spectra have been identified in accordance to the literature.[17]

The high-frequency region (3600–2700 cm^{-1}) contains absorption bands originating mainly from localized CH stretching vibrations.

In the spectral range from 1700 to 1250 cm^{-1}, the two bands centered at 1593 and 1416 cm^{-1} are characteristic of asymmetric and symmetric CO stretching vibrations. The bands centered at 1550 and 1515 cm^{-1} are assigned to a CC stretching vibration of monosubstituted phenyl rings in bipy and dbm ligands. By the analogy with similar compounds,[18] the bands observed at 1477 and 1458 cm^{-1} should correspond to a CC/CN stretching vibration associated with the bipy group. The absorption band at 1395 cm^{-1} involves CC/CN stretching+CH bending vibrations of the dbm fragments. The bands recorded in the IR spectra with peak positions at 1308, 1288 and 1218 cm^{-1} are attributed to in-plane CCH and CCN bending vibrations. In the region below 1200 cm^{-1}, the out-of-plane CCH vibrations are usually observed, with the most intense bands centered around 750-650cm^{-1}. They are assigned to δ(CH) out-of-plane bending vibrations and γ(CH) in-plane ring breathing modes, both from the phenyl groups in the *β*-diketonate and from bipy. The shifts in their respective frequencies (*vs.* those of free ligands) are due to the perturbations induced by the coordination to the Er^{3+} ion.

Finally, vibrations in the region of 700–400 cm^{-1} are to be assigned to ν(Er–O) and ν(Er-N) bonds, in agreement with Tsaryuk *et al.*[19]

Raman spectrum

The Raman spectrum of the complex (see Figure 7) shows a peak at 3071 cm^{-1} and a band centered at ca. 2870 cm^{-1}, which are assigned to $\varphi\upsilon$(CH) and $\upsilon_{as}(CH_3)$, respectively.

The peaks in the 1600-1300 cm^{-1} region are assigned to symmetric and asymmetric ν(C···N), ν(C···O), ν(C···C), ν(C···C···C···O) vibrations from the coordinated bipy molecule and dbm *β*-diketonates (*viz.*, υ(C=C)+υ(C=O) at 1600 cm^{-1}, υ_s(C=C-C=O) at 1540 cm^{-1}, υ_{as}(C-C=C-O) at 1436 cm^{-1} and υ_s(C=C-C=O) at 1316 cm^{-1}).

Those in the 1300-1000 cm^{-1} range are associated to *β*(CH) or *β*(CCC), either alone or combined with ν(CC).

In-plane and out-of-plane ring deformations of the phenyl and chelated rings, C-Ph bending and CH_α out-of-plan bending modes, both from the phenyl groups in the dbm and from bipy, appear below 1000 cm^{-1}. The shifts in their respective frequencies (*vs.* those of free ligands) are due to the perturbations induced by the coordination to the Er^{3+} ion.

In relation to the bands in the 500–100 cm^{-1} region, they can either be ascribed to the neutral ligand (provided that the bands of bipy are only marginally affected by the complexation, displaying small wavenumber shifts or intensity changes[20]) or to the symmetrical and asymmetrical Er–O and Er–N stretching modes. The intense peak at 93 cm^{-1} is to be assigned to ν(CC) from the phenyl groups.

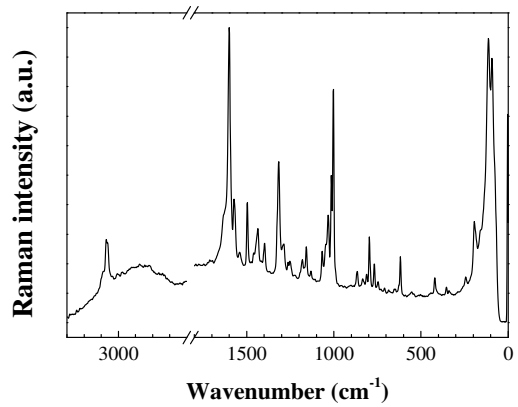

Figure 7. Raman spectrum of [Er(dbm)$_3$(bipy)] complex

Absorption and luminescence

Absorption

The room temperature spectrum derived from diffuse reflectance measurements of the complex in the UV-Vis-NIR range (200-2000 nm) is shown in Figure 8. The broad and intense absorption band in the 200-500 nm range is associated to the organic ligands' π-π* transitions from the S_0 ground state to the S_1 excited state. It consists of several bands centered at 240 nm, 290 nm, 325 nm and 380 nm. The two first peaks are associated to intra-ligand transitions of the 2,2'-bipyridine ligand,[21] while the two later are to be assigned to π→π* transitions in the dbm moiety.[22]

Moreover, sharp peaks associated to intra-configurational $4f^{11}$–$4f^{11}$ electronic transitions starting from the $^4I_{15/2}$ ground state to the different excited levels of the Er^{3+} ion can be discerned. The bands correspond to the transitions from the $^4I_{15/2}$ ground state to $^4F_{7/2}$ (~486.5 nm), $^2H_{11/2}$ (~522 nm), $^4S_{3/2}$ (~544 nm), $^4F_{9/2}$ (~660 nm), $^4I_{9/2}$ (~802 nm), $^4I_{11/2}$ (~977 nm) and $^4I_{13/2}$ (~1532 nm) Er^{3+} excited states.[23] The areas below the band profiles give a qualitative and relative measurement of the absorption probabilities of these Er^{3+} transitions in the $[Er(dbm)_3(bipy)]$ complex. Moreover, these profiles show almost no structure but a broadening, inhomogeneous in nature, that is related to the existence of different local environments for the Er^{3+} ions in the complex with slightly different Er^{3+}-ligands bond distance and angles. Figure 8 also shows the second and third overtones of aromatic C–H stretching vibration, which appear near 1675 nm and 1140 nm, respectively.

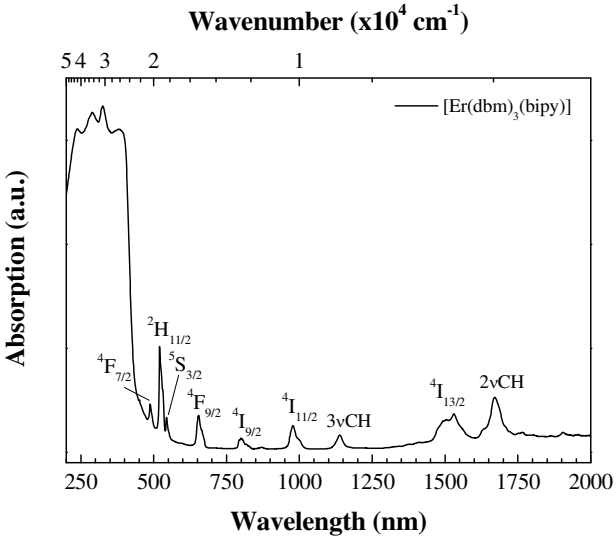

Figure 8. Diffuse reflectance spectrum of the $[Er(dbm)_3(bipy)]$ complex in the UV-visible-NIR range at room temperature. Transitions associated to absorptions of the Er^{3+} ions start from the $^4I_{15/2}$ ground state to the indicated $^{2S+1}L_J$ multiplets.

Photoluminescence

PL in the UV-Vis range. The emission from the Er^{3+} complex in the visible region has been studied under direct excitation of the organic ligands at 280 nm (bipy moiety excitation) and at 405 nm (dbm ligands excitation). In the first case (see Figure 9), we can observe significant reabsorption of the bipy-associated fluorescent emission by the dmb ligand up to ca. 430 nm. On the other hand, upon dbm excitation (see Figure 10), the visible spectrum features an intense broad band which extends up to the red region, associated to residual fluorescent emission, in agreement with Tan *et al.*[24] It should be noted that there are some dips in the emission spectrum that can be readily associated to Er^{3+} ions re-absorption. The diffuse reflectance spectrum of the complex is also plotted in Figure 10 to allow direct comparison.

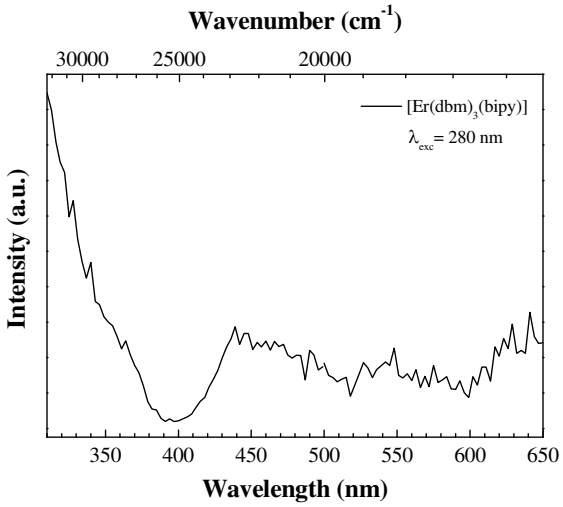

Figure 9. PL emission in the visible region upon excitation at 280 nm (corrected).

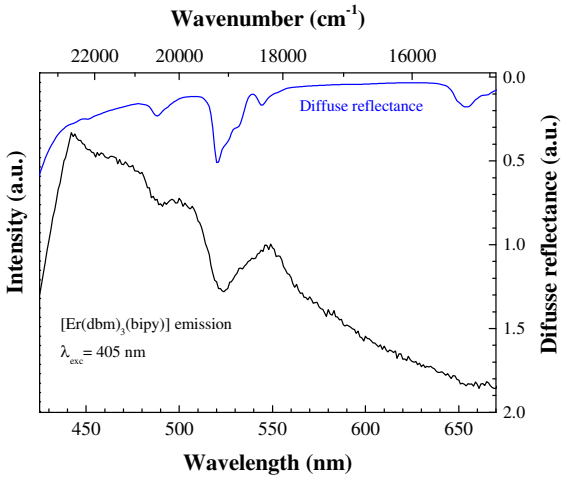

Figure 10. Photoluminescence spectra in the visible region for the $[Er(dbm)_3(bipy)]$ upon excitation at 405 nm.

PL emission in the NIR. The NIR emission spectra for the complex was first recorded using the $S_0 \rightarrow S_1$ excitation band at ca. 380 nm using a Xe lamp (see Figure 11). A broad emission in the near-IR region is obtained, peaking at around 1530 nm, with some structure associated to the Stark energy levels hyperfine structure and the electron population distributions of the $^4I_{13/2}$ and $^4I_{15/2}$ multiplets. As mentioned above, such emission is the result of an efficient energy transfer from the organic ligands to the Er^{3+} ion in the resulting local

environment in the complex under study. The measurements of the NIR emission spectrum upon direct excitation of the $^4I_{9/2}$ state at 800 nm with laser radiation yield the same results (not shown).

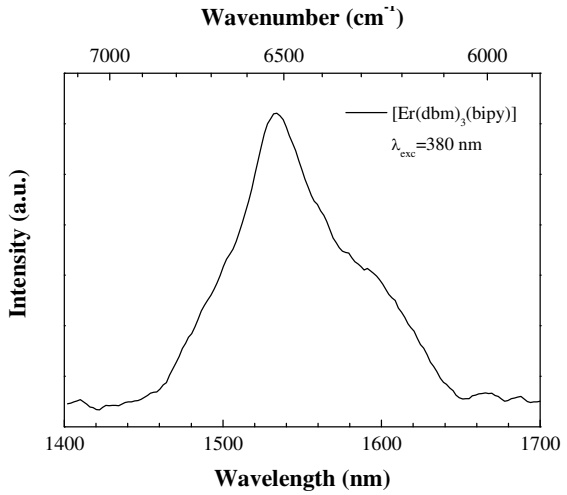

Figure 11. Photoluminescence spectrum in the NIR region upon ligand mediated excitation in the UV region (λ=380 nm)

EXCITATION SPECTRUM

The UV-VIS excitation spectrum has been recorded in the 280-500 nm region at room temperature monitoring the NIR emission of Er^{3+} at 1530 nm (see Figure 12). The spectrum features an intense broad band, in agreement with the UV-Vis absorption spectrum and with the excitation spectra reported elsewhere,[15a,15c] which corresponds to the intra-ligand singlet-singlet π-π* electronic transition of the dibenzoylmethane ligand. This energy absorption in the UV-Vis region by the *β*-diketonate ligand is adequate to sensitize the metal-centered emitting states, leading to intense characteristic Er^{3+} luminescence in the NIR range.

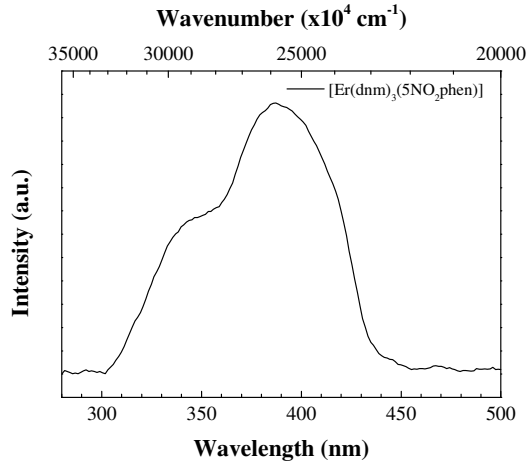

Figure 12. Excitation spectrum of the $^4I_{13/2} \rightarrow {}^4I_{15/2}$ emission (λ_{em}=1530 nm) of Er^{3+} in [Er(dbm)$_3$(bipy)] at RT.

LIFETIME MEASUREMENTS

As the excitation measurements indicate that dbm moeity is the ligand structure responsible for the ligand to metal energy transfer process, the decay of the ligand fluorescence has been measured when the 405 nm excitation pump laser is used to selectively excite the dbm molecules. The detection wavelength was tuned at the maximum of the emission band, around 460 nm. However, the decay of the ligand fluorescence can hardly be distinguished from the instrumental response function (IRF) curve, which shows the temporal width of the pump laser. This means that the decay of the dbm fluorescence is beyond the temporal resolution of the equipment, which is estimated to be about 0.07 ns.

Moreover, the observed fast decay of the ligand fluorescence is a further indication of the resonant energy transfer from the ligand to the metal, which explains the UV excitation spectrum and the intense IR emission of Er^{3+} ions under pumping of the ligand counterpart.

The NIR PL decay of the $^4I_{13/2}$ multiplet was measured both upon ligand-mediated excitation (at 380 nm) and upon direct excitation of the Er^{3+} ions (at 520 nm) with an OPO laser at 10 Hz repetition rate. The decay shows a single exponential behavior, which can be observed as a linear dependence in the semi-log representations of Figure 13. The good fitting to a single-exponential function confirms a unique and consistent coordination environment around the lanthanide ion.[25] The $^4I_{13/2}$ lifetime value for the complex is τ=1.1 μs, which is similar to other Er^{3+} complexes previously reported by other authors[26]. Taking into account that the radiative lifetime (τ_{rad}) of Er^{3+} is ca. τ=2-3 ms, the quantum efficiency of these compounds is $\eta=\tau/\tau_{rad}$~0.1%. Nonetheless, these lifetime values are known to increase when the complexes are dispersed in a suitable host matrix: for example, in poly(methyl methacrylate) (PMMA), values in the ms range have been reported for analogous complexes: τ_{rad}=7.665 ms for [Er(dbm)$_3$(TPPO)$_2$];[5a] τ_{rad}=5.33 ms[5b] and τ_{rad}=6.698 ms[5c] for [Er(dbm)$_3$(phen)], close to the emission decay time of the isolated ion, τ=8 ms.

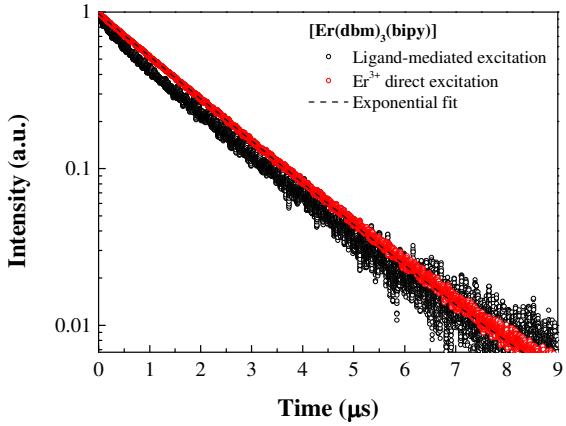

Figure 13. Room temperature PL decay of the $^4I_{13/2}$ multiplet measured under ligand excitation at 380 nm (*black*) and upon direct excitation of Er^{3+} at 520 nm (*red*). The single-exponential fit is also included (*dashed black line*).

Magnetic measurements

The temperature dependence of the magnetization was measured in the temperature range 5-300 K under a field of 100 Oe. As expected this compound shows paramagnetic behaviour, and its $\chi_M T$ product drops from 11.75 emu·K·mol^{-1} at 300 K to 6.5 emu·K·mol^{-1} at 5 K (Figure 14). At 300 K the effective magnetic moment is 9.7 μ_B, very close to the expected value of 9.6 μ_B for a non-interacting Er^{3+} ion ($^4I_{15/2}$, and g=6/5). The gradual decrease of $\chi_M T$ upon cooling can be understood as resulting from a progressive depopulation of excited Stark sublevels due to the ligand field, suggesting the presence of significant magnetic anisotropy as commonly observed in lanthanide compounds. The $\chi_M T$ value at 5 K is very similar to other Er^{3+} β-diketonate complexes already reported.[7a,7b] The inset of Figure 14 shows the magnetic field dependences of magnetization at 1.8, 5 and 10 K, measured up to 5 T with a sweeping rate of 0.6 T/min. Down to 1.8 K the compound did not show any magnetic hysteresis. At this temperature and up to 5 T, magnetization approaches a value of 5.8 μ_B, still far from the expected saturation value for a free Er^{3+} ion. This fact can also be explained by the magnetic anisotropy of the compound.

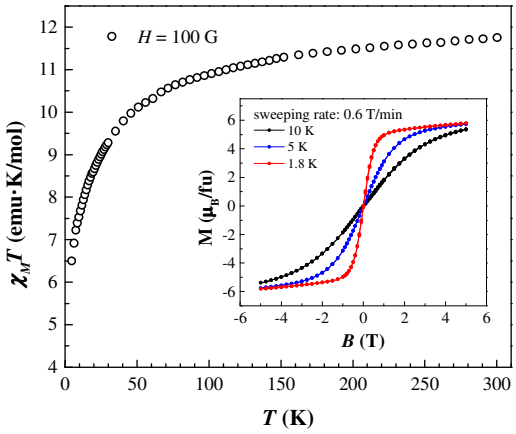

Figure 14. Static magnetic properties of the [Er(dbm)$_3$(bipy)] complex: plot of μ_{eff} in the 4.8-300 K range and H_{DC}=100 Oe. *Inset*: Hysteresis loops at different temperatures with a sweeping rate of 0.6 T/min.

Similarly to other reported Er^{3+} β-diketonate complexes,[7a,7b] the magnetization dynamics of [Er(dbm)$_3$(bipy)] were investigated by alternating current (AC) susceptibility measurements in zero and higher static DC fields. In the low temperature range 1.7–10 K and zero magnetic field, no maxima in both components of the AC susceptibility, in-phase, χ', and out-of-phase, χ", are observed (Figure 15). On the contrary, the application of a DC field of 1000 Oe drastically changes the relaxation dynamics, as shown in Figure 16, with both χ' and χ" components presenting maxima with strong frequency dependence and an increase of the χ' to χ'' ratio. This behaviour clearly denotes the presence of fast zero-field tunneling of the magnetization between sub-levels, which is suppressed with the application of the static DC field.

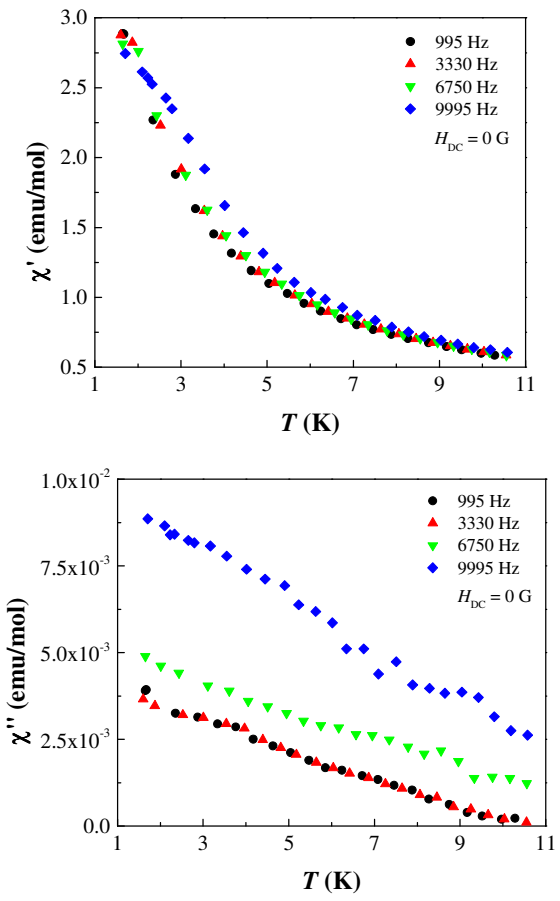

Figure 15. In-phase (*top*) and out-of-phase (*bottom*) components of the AC susceptibility at different frequencies in the 1.7–11 K temperature range for [Er(dbm)$_3$(bipy)] complex. H_{AC}=5 Oe; H_{DC}=0 Oe.

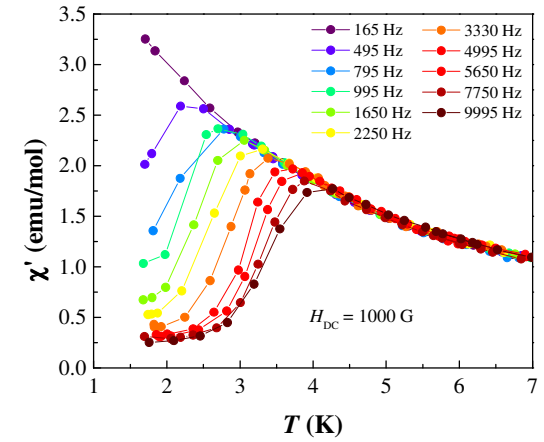

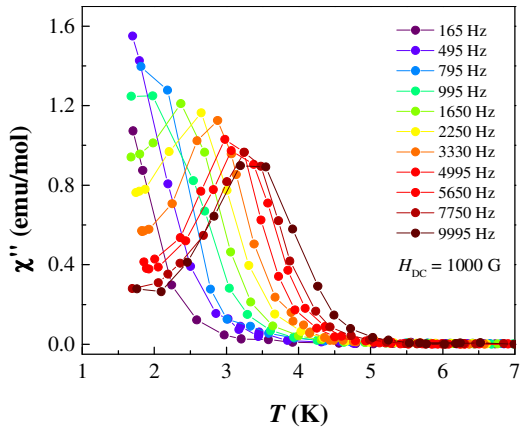

Figure 16. In-phase (*top*) and out-of-phase *(bottom)* components of the AC susceptibility at different frequencies in the 1.7–7 K temperature range for $[Er(dbm)_3(bipy)]$ complex. H_{AC}=5 Oe; H_{DC}=1000 Oe.

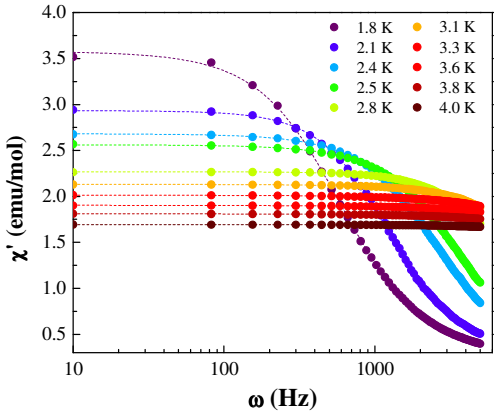

Figure 17. In-phase (*top*) and out-of-phase *(bottom)* components of the AC susceptibility at different temperatures in the 10–10 kHz frequency range range for $[Er(dbm)_3(bipy)]$ complex. Debye fittings are shown as dashed lines. H_{AC}=5 Oe; H_{DC}=1000 Oe.

The magnetization relaxation rate was probed in the temperature range 1.6 to 5 K by measuring χ' and χ'' at fixed temperatures while the frequency, ω, of the AC field was varied from 10 Hz to 10 kHz (Figure 17). These data provided Cole-Cole plots (χ'' *vs.* χ' plots) for those different temperatures that were fitted with the generalized Debye model,[27] $\chi(\omega) = \chi_S+(\chi_T+\chi_S)/(1+i\omega\tau)^{1-\alpha}$, where χ_S and χ_T are the adiabatic and isothermal susceptibilities, τ is the average magnetization relaxation time, and α is a parameter ranging from 0 to 1 which quantifies the width of the relaxation time distribution ($\alpha = 0$ corresponds to the ideal Debye model, with a single relaxation time). Figure 18 *(left)* shows the Cole-Cole plots obtained under a DC field of 1000 Oe. The small α values obtained (see Table 3), along with the nearly semi-circular and symmetrical shape of the Cole-Cole plots, support the existence of a single relaxation process.

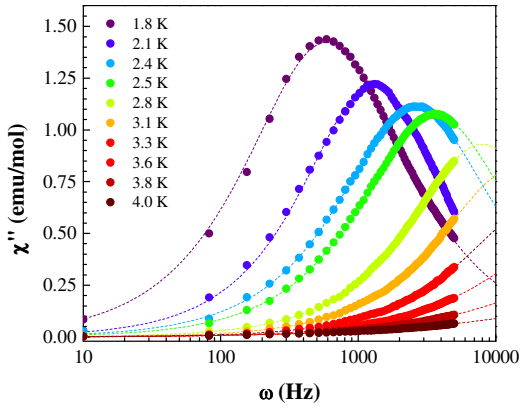

When plotted with the correspondent inverse of temperature, these single relaxation times τ have an activated temperature dependence (Figure 18 *right*) that follows an Arrhenius law, $\tau(T) = \tau_0 \cdot \exp(E_{eff}/k_BT)$ in the higher temperature range (dashed line), with a pre-exponential factor $\tau_0 = 1.73\times10^{-8}$ s and an effective relaxation barrier of E_{eff} = 26.8 K, which is higher when compared with complex $[Er(h)_3(bipy)]$[7a] [8 K] or complex $[Er(tfa)_3(bipy)$ [15 K] and quite distinct from complex $[Er(tpm)_3(bipy)]$, which exhibits two thermally activated processes with energy barriers of 9 and 40K.[7c] A correlation with structural parameters α and ϕ discussed in the structural section above is quite difficult; only further DFT calculations may shed some light on the diversity of results.[28] $[Er(dbm)_3(bipy)]$ energy barrier is within the range of most of other well-known *d*-[29] and *f*-element SMMs.[7a,7b,30] In the lower temperature range, some deviation from this activated regime is noticed, likely due to the approaching of a quantum tunneling regime.

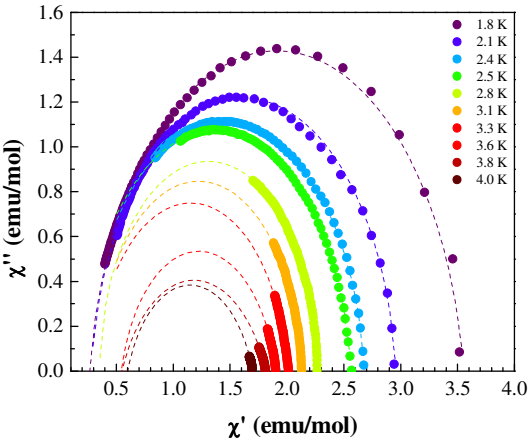

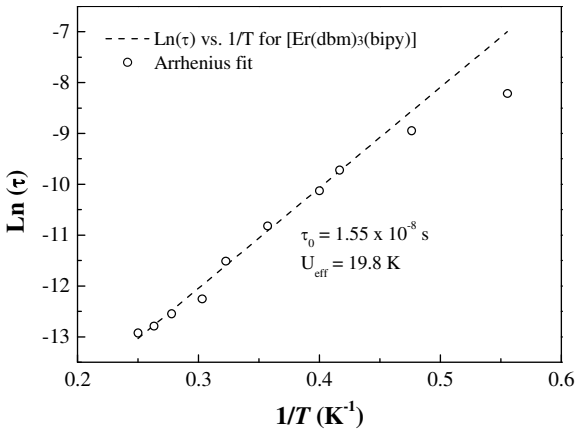

Figure 18. *(top)* Argand diagrams and Debye fittings for $[Er(dbm)_3(bipy)]$ complex. H_{AC}=5 Oe; H_{DC}=1000 Oe; *(bottom)* Arrhenius Law fitting for $[Er(dbm)_3(bipy)]$ complex. H_{AC}=5 Oe, H_{DC}=1000 Oe.

Table 3. Debye model fitting parameters from 1.6 to 4.8 K for $[Er(dbm)_3(bipy)]$.

$[Er(dbm)_3(bipy)]$ H_{DC} = 1000 G				
T (K)	χ_S	χ_T	τ (s)	α
1.8	0.263	3.556	2.7×10^{-4}	0.090
2.1	0.280	2.957	1.3×10^{-4}	0.060
2.4	0.223	2.680	6.0×10^{-5}	0.062
2.5	0.185	2.562	4.0×10^{-5}	0.074
2.8	0.353	2.267	2.0×10^{-5}	0.035
3.1	0.320	2.130	1.0×10^{-5}	0.061
3.3	0.300	2.009	4.8×10^{-6}	0.137
3.6	0.545	1.905	3.6×10^{-6}	0.152
3.8	0.550	1.817	2.8×10^{-6}	0.162
4.0	0.600	1.700	2.44×10^{-6}	0.2247

Conclusions

A new Er^{3+} complex with dibenzoylmethane β-diketonate ligand and 2,2'-bipyridine diimide, $[Er(dbm)_3(bipy)]$, has been synthesized and its structural, thermal, luminescent and magnetic properties have been studied.

The material combines luminescence along with a magnetic relaxation at low temperature: upon excitation in the UV at 380 nm, efficient ligand-mediated sensitization is attained by antenna effect, leading to NIR emission at 1.53 μm from the $^4I_{13/2}\rightarrow{}^4I_{15/2}$ transition of Er^{3+} ion, which has practical applications in areas such as labeling, biological analysis and optoelectronics. In addition, its SIM behavior, with a 19.8 K thermally activated barrier upon the application of a 1000 Oe static field, opens up a popular avenue to nanoscale electronic devices, sensors and high-density data storage media at the molecular level.

Experimental

Materials, synthesis and analytical data

All reagents and solvents employed were commercially available and used as supplied without further purification. All the procedures for complex preparation were carried out under nitrogen and using dry reagents to avoid the presence of water and oxygen, which can quench metal photoluminescence.

Tris(dibenzoylmethanate)mono(2,2´-bipyridine)erbium(III), $[Er(dbm)_3(bipy)]$, was synthesized as follows: under stirring, a dibenzoylmethane (3 mmol) methanol solution (20 mL) was added to 1 mmol of $Er(NO_3)_3{\cdot}5H_2O$ in methanol. The mixture was neutralized by adding potassium methoxide (3 mmol) dropwise under vigorous stirring until potassium nitrate precipitated. KNO_3 was removed by decanting, and 2,2'-bipyridine (1 mmol) was finally added. The mixture was heated to 75 ºC and stirred overnight, then washed with dioxane, and finally dried in vacuum to give product in 90-95% yield (based on Er). Crystals suitable for X-ray analysis were obtained by slow evaporation of a methanol-dioxane solution at room temperature (RT).

$[Er(dbm)_3(bipy)]$: Chemical formula: $C_{55}H_{41}ErN_2O_6$, M_W: 993.18. Anal. Calcd. for $C_{55}H_{41}ErN_2O_6$: C, 66.51; H, 4.16; Er, 16.84; N, 2.82; O, 9.67%. Found: C, 66.42; H, 4.20; N, 2.88%.

X-ray crystallographic analysis

Prior to structural characterisation, a powder diffractogram of the complex was obtained using a Bruker D8 Advance Bragg-Brentano diffractometer, in reflection geometry.

For the determination of the crystal structure by X-ray diffraction, a crystal of the aforementioned compound was glued to a glass fibre and mounted on a Bruker APEX II diffractometer. Diffraction data was collected at room temperature 293(2) K using graphite monochromated MoKα (λ=0.71073 Å). Absorption corrections were made using SADABS.[31] The structure was solved by direct methods using SHELXS-97[32] and refined anisotropically (non-H atoms) by full-matrix least-squares on F^2 using the SHELXL-97 program.[32] PLATON[13] was used to analyse the structure. The solvated form contains large enough voids to accommodate solvent molecules (probably 1,4-dioxane). These molecules were found to be heavily disordered. The disordered electron density, was treated with the SQUEEZE routine in PLATON. The formula mass and density do not take the solvent into account. Mercury, version 3.3[33] was used for figure plotting. Atomic coordinates, thermal parameters and bond lengths and angles have been deposited at the Cambridge Crystallographic Data Centre (CCDC). Any request to the CCDC for this material should quote the full literature citation and the reference numbers CCDC 1027090 and 1027091.

Physical and optical measurements

The C, H, N elemental analyses were conducted using a Perkin Elmer CHN 2400 apparatus.

Differential scanning calorimetry (DSC) data were obtained on a DSC Pyris1 Perkin Elmer instrument, equipped with an intracooler cooling unit at -25 ºC (ethylene glycol-water, 1:1 v/v, cooling mixture), with a heating rate β=10°C/min, under a N_2 purge, 20 mL/min. Infrared spectra were recorded with a Thermo Nicolet 380 FT-IR apparatus equipped with Smart Orbit Diamond ATR system. Raman spectra were recorded with a FT-Raman Bruker FRA106 by using a near-IR (Nd: YAG, 1064.1 nm) laser to excite the samples.

The UV-Vis-NIR diffuse reflectance spectrum of the material in the range from 200 to 2000 nm was measured using an integrating sphere coupled to a spectrophotometer (Agilent Cary 5000) in powder form.

The photoluminescence (PL) spectra in the UV-Vis region were obtained using a 280 nm picosecond pulsed light emitting diode (Edinburgh Instruments EPLED-280), with a typical pulse width of 700 ps, and a 405 nm picosecond pulsed diode laser (Edinburgh Instruments EPL-405), with a typical pulse width of 80 ps. The later was also used for the ligand fluorescence decay measurements. The emission spectra and the ligand fluorescence decay were recorded using a fluorescence spectrometer with a single photon counting multichannel plate photomultiplier and a dedicated acquisition software (Edinburgh Instruments LifeSpec II and F900 software). The NIR PL spectrum was measured exciting the sample using either the 800 nm radiation of a cw Ti:sapphire laser (Spectra Physics 3900S) pumped by a 10 W cw Ar^+ laser (Spectra Physics 2060-10 Beamlock) or a 450 W Xenon arc lamp followed by a 0.22 m double-grating monochromator (Spex 1680) to provide an excitation beam centred at 380 nm. The NIR emission was focused with a convergent lens onto a 0.18 m single-grating monochromator (Jobin Yvon Triax180, grating 600 grooves/mm, blaze 1.0 μm) with a resolution of 0.5 nm and then detected with a Peltier-cooled InGaAs photodiode (Hamamatsu pin G5851-21) at -25 ºC. For the excitation spectra, a Xenon arc lamp with a 1/8 m monochromator (Oriel 77250) was used, detecting the emission at a fixed wavelength (1540 nm) using the NIR emission setup. The NIR luminescence decay curves were measured both upon excitation of the ligands at 380 nm and upon direct excitation of Er^{3+} ions at 520 nm with an OPO (Continuum Panther OPO, Laser Photonics) pumped with a Nd-YAG (Surelite) [pulse width: 7 ns; frequency: 10 Hz]. The emitted light was dispersed with a 0.55 m single-grating monochromator (Jobin Yvon Triax550, grating 600 grooves/mm) and detected with a liquid nitrogen-cooled photomultiplier (Hamamatsu R5509-72) and a lock-in amplifier (7265 DSP Perkin Elmer). The lifetime was measured by using a digital oscilloscope (LeCroy 500 MHz). All spectra were measured at room temperature and corrected for the spectral response of the equipment, and samples were analysed directly as powder.

The magnetic susceptibility under several magnetic fields was measured with a SQUID magnetometer (S700X, Cryogenic Ltd) in the temperature range 4-300 K and assuming a diamagnetic contribution estimated from tabulated Pascal constants of -5.91×10^{-4} emu·mol^{-1}. Field dependence of the magnetization was measured up to 5 T at different fixed temperatures from 1.7 K to 10 K. AC measurements were taken using a MagLab 2000 system (Oxford Instruments). Temperature dependence of AC magnetic susceptibility was measured in the 10-10^4 Hz frequency range under a zero and 10^3 Oe static DC field. Additional isothermal AC susceptibility measurements, $\chi_{AC}=f(\omega)$,were taken in the 10-10^4 Hz frequency range, within 1.7 and 5 K.

Acknowledgements

The authors gratefully acknowledge Dr. I. Hernández-Campo (CITIMAC, University of Cantabria) for conducting the NIR lifetime measurements. P. Martín-Ramos would like to thank Iberdrola Foundation for its financial support. J.T. Coutinho acknowledges the support by FCT under the scholarship SFRH/BD/84628/2012. Support by MICINN (MAT2010-21270-C04-02, MAT2013-46649-C4-4-P, the Consolider-Ingenio 2010 Program MALTA CSD2007-00045 and the Spanish National Program of Infrastructure), Caja-Canarias Foundation (ENER01), and by EU-FEDER funds are gratefully acknowledged by La Laguna group. CEMDRX group is grateful to Fundação para a Ciência e a Tecnologia (FCT) for providing funds under grant PEst-C/FIS/UI0036/2011. UVa group acknowledges financial support of Junta de Castilla y León through project VA300A12-1.

Notes and references

[a] CEMDRX, Physics Department, Universidade de Coimbra, Rua Larga, P-3004-516 Coimbra, Portugal.

[b] Advanced Materials Laboratory, ETSIIAA, Universidad de Valladolid, Avenida de Madrid 44, 34004 Palencia, Spain.

[c] Solid State Group, UCQR, IST/CTN, Instituto Superior Técnico, UTL, Estrada Nacional 10, km 139.7, 2695-066 Bobadela LRS, Portugal.

[d] Department of Physics, MALTA Consolider Team, and Institute of Advances Studies in Atomic, Molecular and Photonics. Universidad de La Laguna, E-38200 San Cristóbal de La Laguna, Santa Cruz de Tenerife, Spain.

† Electronic Supplementary Information (ESI) available: CCDC 1027090 and 1027091 contain the supplementary crystal data for $[Er(dbm)_3(bipy)]$ and its solvated form. For crystallographic data in CIF or other electronic format see DOI: 10.1039/b000000x/

1. (a) E. Brunet, O. Juanes and J. C. Rodriguez-Ubis, *Current Chemical Biology*, 2007, **1**, 11-39; (b) S. Comby and J.-C. G. Bünzli, in *Optical Spectroscopy*, eds. V. K. Pecharsky, J. C. G. Bünzli and K. A. Gschneider, Jr., Elsevier, 2007, pp. 217-470.
2. J.-M. Lehn, *Angew. Chem. Int. Ed.*, 1990, **29**, 1304-1319.
3. (a) K. Binnemans, in *Handbook on the Physics and Chemistry of Rare Earths*, eds. K. A. Gschneidner, J.-C. G. Bünzli and V. K. Pecharsky, Elsevier B.V., North-Holland, 2005, vol. 35, pp. 107-272; (b) P. Li, Y. Wang, H. Li and G. Calzaferri, *Angew. Chem. Int. Ed.*, 2014, **53**, 2904-2909; (c) X. Chen, P. Zhang, T. Wang and H. Li, *Chemistry – A European Journal*, 2014, **20**, 2551-2556; (d) H. Wang, Y. Wang, L. Zhang and H. Li, *RSC Adv.*, 2013, **3**, 8535-8540.
4. Y. Kawamura, Y. Wada and S. Yanagida, *Jpn. J. Appl. Phys.*, 2001, **40**, 350-356.
5. (a) H. Liang, B. Chen and Z. Zheng, *physica status solidi (b)*, 2004, **241**, 3056-3061; (b) H. Liang, Z. Zheng, B. Chen, Q. Zhang and H. Ming, *Mater. Chem. Phys.*, 2004, **86**, 430-434; (c) Z. Zheng, H. Liang, H. Ming, Q. Zhang and J. Xie, *Opt. Commun.*, 2004, **233**, 149-153; (d) L.-N. Sun, H.-J. Zhang, C.-Y. Peng, J.-B. Yu, Q.-G. Meng, L.-S. Fu, F.-Y. Liu and X.-M. Guo, *The Journal of Physical Chemistry B*, 2006, **110**, 7249-7258; (e) B. Tong, S. Wang, Y. Meng and B. Wang, *Photochemical & Photobiological Sciences*, 2007, **6**, 519-520.

6. (a) F. X. Zang, Z. R. Hong, W. L. Li, M. T. Li and X. Y. Sun, *Appl. Phys. Lett.*, 2004, **84**, 2679-2681; (b) D. Zhang, W. Li, B. Chu, X. Li, L. Han, J. Zhu, T. Li, D. Bi, D. Yang, F. Yan, H. Liu and D. Wang, *Appl. Phys. Lett.*, 2008, **92**, -; (c) H. S. Guan, C. H. Cheng, W. C. Li, D. F. Geng and Z. Q. Fan, *Chemical Research in Chinese Universities*, 2009, **25**, 786-790; (d) F. Zang, S. Tze-Chien, F. Zhu, H. Zi-Ruo, S. Xiaoyan, W.-l. Li and C. H. A. Huan, *Lightwave Technology, Journal of*, 2009, **27**, 1522-1526; (e) F. Wei, Y. Z. Li, G. Z. Ran and G. G. Qin, *Opt. Express*, 2010, **18**, 13542.
7. (a) M. Ramos Silva, P. Martín-Ramos, J. T. Coutinho, L. C. J. Pereira and J. Martín-Gil, *Dalton Trans.*, 2014, **43**, 6752; (b) P. Martín-Ramos, M. Ramos Silva, J. T. Coutinho, L. C. J. Pereira, P. Chamorro-Posada and J. Martín-Gil, *Eur. J. Inorg. Chem.*, 2014, **2014**, 511-517; (c) M. Ramos Silva, P. Martín-Ramos, J. T. Coutinho, L. C. J. Pereira, V. Lavín, I. R. Martín, P. S. Pereira Silva and J. Martín-Gil, *Dalton Trans.*, 2014, **Accepted, pending minor revision**.
8. (a) S.-D. Jiang, B.-W. Wang, H.-L. Sun, Z.-M. Wang and S. Gao, *J. Am. Chem. Soc.*, 2011, **133**, 4730-4733; (b) K. R. Meihaus and J. R. Long, *J. Am. Chem. Soc.*, 2013, **135**, 17952-17957; (c) J.-L. Liu, Y.-C. Chen, Y.-Z. Zheng, W.-Q. Lin, L. Ungur, W. Wernsdorfer, L. F. Chibotaru and M.-L. Tong, *Chem. Sci.*, 2013, **4**, 3310-3316; (d) L. Ungur, J. J. Le Roy, I. Korobkov, M. Murugesu and L. F. Chibotaru, *Angew. Chem. Int. Ed.*, 2014, **53**, 4413-4417; (e) J. J. Le Roy, I. Korobkov and M. Murugesu, *Chem Commun (Camb)*, 2014, **50**, 1602-1604.
9. M. N. Leuenberger and D. Loss, *Nature*, 2001, **410**, 789-793.
10. E. Chelebaeva, J. Larionova, Y. Guari, R. A. Ferreira, L. D. Carlos, F. A. Paz, A. Trifonov and C. Guerin, *Inorg. Chem.*, 2008, **47**, 775-777.
11. (a) B. V. Harbuzaru, A. Corma, F. Rey, P. Atienzar, J. L. Jordá, H. García, D. Ananias, L. D. Carlos and J. Rocha, *Angew. Chem. Int. Ed.*, 2008, **47**, 1080-1083; (b) S. Mohapatra, B. Rajeswaran, A. Chakraborty, A. Sundaresan and T. K. Maji, *Chem. Mater.*, 2013, **25**, 1673-1679.
12. J. J. Baldoví, E. Coronado, A. Gaita-Ariño, C. Gamer, M. Giménez-Marqués and G. Mínguez Espallargas, *Chem. Eur. J.*, 2014, **20**, 10695-10702.
13. A. L. Spek, *J. Appl. Crystallogr.*, 2003, **36**, 7-13.
14. L. Sorace, C. Benelli and D. Gatteschi, *Chem. Soc. Rev.*, 2011, **40**, 3092.
15. (a) A. K. Singh, S. K. Singh, H. Mishra, R. Prakash and S. B. Rai, *The Journal of Physical Chemistry B*, 2010, **114**, 13042-13051; (b) X. Li, G. Xiao, H. Chi, Y. Dong, H. Zhao, P. Lei, Z. Zhang, Z. Hu, S. Wu, Z. Su and W. Li, *Mater. Chem. Phys.*, 2010, **123**, 289-292; (c) Y. Liu, Y. Wang, H. Guo, M. Zhu, C. Li, J. Peng, W. Zhu and Y. Cao, *J. Phys. Chem. C*, 2011, **115**, 4209-4216; (d) S. Li, *Luminescence*, 2012, **27**, 242-245.
16. D. Zhou, C. Huang, G. Yao, J. Bai and T. Li, *J. Alloys Compd.*, 1996, **235**, 156-162.
17. (a) S. F. Tayyari, H. Rahemi, A. R. Nekoei, M. Zahedi-Tabrizi and Y. A. Wang, *Spectrochimica Acta Part A: Molecular and Biomolecular Spectroscopy*, 2007, **66**, 394-404; (b) K. Nakamoto, *Infrared and Raman Spectra of Inorganic and Coordination Compounds, Applications in Coordination, Organometallic, and Bioinorganic Chemistry*, 6th edn., Wiley, 2009; (c) A. R. Nekoei, M. Vakili, M. Hakimi-Tabar, S. F. Tayyari, R. Afzali and H. G. Kjaergaard, *Spectrochimica Acta Part A: Molecular and Biomolecular Spectroscopy*, 2014, **128**, 272-279.
18. G. Dovbeshko, O. Fesenko, R. Fedorovich, T. Gavrilko, A. Marchenko, G. Puchkovska, L. Viduta, A. Naumovets, D. Chubich, A. Vitukhnovskii and D. Fichou, *J. Mol. Struct.*, 2006, **792-793**, 115-120.
19. V. Tsaryuk, V. Zolin, J. Legendziewicz, R. Szostak and J. Sokolnicki, *Spectrochim. Acta, Pt. A: Mol. Biomol. Spectrosc.*, 2005, **61**, 185-191.
20. (a) José A. Fernandes, Rute A. S. Ferreira, M. Pillinger, Luís D. Carlos, Isabel S. Gonçalves and Paulo J. A. Ribeiro-Claro, *Eur. J. Inorg. Chem.*, 2004, **2004**, 3913-3919; (b) J. A. Fernandes, R. A. Sá Ferreira, M. Pillinger, L. D. Carlos, J. Jepsen, A. Hazell, P. Ribeiro-Claro and I. S. Gonçalves, *J. Lumin.*, 2005, **113**, 50-63.
21. L. N. Puntus, K. A. Lyssenko, I. S. Pekareva and J.-C. G. Bünzli, *The Journal of Physical Chemistry B*, 2009, **113**, 9265-9277.
22. (a) J.-C. Hubaud, I. Bombarda, L. Decome, J.-C. Wallet and E. M. Gaydou, *J. Photochem. Photobiol. B: Biol.*, 2008, **92**, 103-109; (b) J. Zawadiak and M. Mrzyczek, *Spectrochimica Acta Part A: Molecular and Biomolecular Spectroscopy*, 2012, **96**, 815-819.
23. C. Görller-Walrand and K. Binnemans, in *Handbook on the physics and chemistry of rare earths*, eds. K. A. Gschneidner and L. Eyring Elsevier BV, Amsterdam, 1998, vol. 25, pp. 101-264.
24. C. Tan and Q. Wang, *Synth. Met.*, 2012, **162**, 1416-1420.
25. S. Gago, J. A. Fernandes, J. P. Rainho, R. A. Sá Ferreira, M. Pillinger, A. A. Valente, T. M. Santos, L. D. Carlos, P. J. A. Ribeiro-Claro and I. S. Gonçalves, *Chem. Mater.*, 2005, **17**, 5077-5084.
26. (a) Z. Li, J. Yu, L. Zhou, H. Zhang, R. Deng and Z. Guo, *Org. Electron.*, 2008, **9**, 487-494; (b) X. Li, Z. Si, C. Pan, L. Zhou, Z. Li, X. Li, J. Tang and H. Zhang, *Inorg. Chem. Commun.*, 2009, **12**, 675-677.
27. D. Huser, A. J. v. Duyneveldt, G. J. Nieuwenhuys and J. A. Mydosh, *Journal of Physics C: Solid State Physics*, 1986, **19**, 3697-3717.
28. S. K. Singh, T. Gupta and G. Rajaraman, *Inorg. Chem.*, 2014, 140926111326003.
29. (a) M. Bal, J. R. Friedman, E. M. Rumberger, S. Shah, D. N. Hendrickson, N. Avraham, Y. Myasoedov, H. Shtrikman and E. Zeldov, *J. Appl. Phys.*, 2006, **99**, 08D103; (b) W. H. Harman, T. D. Harris, D. E. Freedman, H. Fong, A. Chang, J. D. Rinehart, A. Ozarowski, M. T. Sougrati, F. Grandjean, G. J. Long, J. R. Long and C. J. Chang, *J. Am. Chem. Soc.*, 2010, **132**, 18115-18126.
30. X.-L. Wang, L.-C. Li and D.-Z. Liao, *Inorg. Chem.*, 2010, **49**, 4735-4737.
31. G. Sheldrick, *SADABS*, (1996) University of Göttingen, Göttingen, Germany.
32. G. M. Sheldrick, *Acta Crystallogr. Sect. A: Found. Crystallogr.*, 2007, **64**, 112-122.
33. C. F. Macrae, P. R. Edgington, P. McCabe, E. Pidcock, G. P. Shields, R. Taylor, M. Towler and J. van de Streek, *J. Appl. Crystallogr.*, 2006, **39**, 453-457.

